ISSN : 2541 - 0318 [Online]
ISSN : 2541 - 2884 [Print]

Numerical Investigation of Steel Section Remaining Tensile Capacity During SMAW Welding

[*] **Malik Mushthofa**[1]
[1] Civil Engineering,Islamic University of Indonesia, Indonesia,Kaliurang St No.Km. 14,5, Ngemplak, Sleman Regency, Special Region of Yogyakarta 55584
malik.mushthofa@uii.ac.id

Abstract
This study investigates a method for calculating the remaining axial tension capacity of thin steel sections during Shielded Metal Arc Welding (SMAW) under load. This necessitates a method to address situations where welding operations must be performed on structures already experiencing stress. Thin sections are particularly susceptible to the elevated temperatures associated with welding. To address this challenge, simulations were utilized to model the effect of the welding heat on thin sections. The simulations considered the temperature rise experienced by each segment within the section. This rise led to a reduction in yield strength, ultimate strength, and elastic modulus for each segment. Subsequently, the partial tension capacity for each segment was calculated based on its area and the reduced strength properties. Finally, the remaining axial tension capacity was determined by summing the tension capacities of all segments. The results revealed a noteworthy correlation between welding parameters and the remaining tension capacity. Higher welding currents were associated with a greater loss of tension capacity, while faster welding speeds resulted in minimizing this loss. The scenario employing the lowest welding current and highest welding speed yielded the most favorable outcome, with the remaining tension capacity reaching 76%, 85%, and 89% for sections of 40.40.4, 50.50.5, and 60.60.6, respectively. Conversely, employing the highest welding current and slowest welding speed significantly reduced the remaining axial tension capacity until there were only 28%, 50%, and 66% left for the respective sections.

Keywords: SMAW welding, tension capacity, welding current, elevated temperature, welding speed

INTRODUCTION

Welding is a crucial process in the construction of steel structures, but it can pose challenges when performed on elements under load. This fact is particularly important for steel frame structures, as they often utilize thin steel sections. The heat generated during welding creates a heat-affected zone (HAZ) around the weld, which experiences elevated temperatures compared to the surrounding material (Parmar & Dubey, (2017), Lozano et al., (2018)). This increase in temperature leads to a reduction in the yield strength and elastic modulus of the steel within the HAZ (Shaiful et al., 2015). For a given welding process and heat input, thinner sections of steel will experience a wider heat-affected zone (HAZ) due to the increased ease of heat transfer through the material (Mushthofa et al., 2023).

When welding on loaded steel structures, the heat-affected zone (HAZ) with its reduced strength can compromise the structural integrity of the member. The reduced strength and stiffness can cause localized deformation and even failure as the load is transferred through the HAZ. This is especially concerning in critical load-bearing members, where any compromise in structural integrity can have catastrophic consequences.

In steel frame structures, the load-carrying ability of individual members is primarily determined by their axial capacity, which can be either in compression or tension. The tensile capacity of a member directly depends on its cross-sectional area, considering both the gross and effective areas. Furthermore, the yield strength and tensile strength of the steel used also affect the tensile capacity. All these factors (cross-sectional area, yield strength, and tensile strength) are variables that are impacted by the cross-section of the member during the welding process.

Due to the reduction in tensile strength caused by SMAW welding, it is essential to identify the extent of this weakening for various cross-sections of steel frame members. This evaluation is particularly critical when welding is performed on loaded structures. By understanding the impact of welding on the members' tensile capacity, engineers can ensure that the remaining strength is sufficient to meet design requirements and maintain the structural integrity of the frame.

While past research has focused heavily on the strength of welded joints themselves (Bi et al., 2022) and their post-welding performance (Zhang et al., 2024), there's a lack of understanding about how these welded members behave when they're under load, particularly during the high temperatures of a fire (Qi et al., 2024). Existing studies on fire resistance often look at the entire structure's response, not the specific behavior of the welded parts themselves (Zhang et al., 2021). This research aims to fill this gap by investigating what happens to welded members when they experience both load and high temperatures at the same time.

Evaluating the reduction in tensile capacity necessitates considering changes within the heat-affected zone (HAZ) to the member's cross-sectional area, yield strength, and tensile strength. These changes are influenced by various factors, including welding parameters (voltage, current, welding speed, electrode diameter, and type) as well as the thickness of the steel section. Therefore, this paper aims to investigate the remaining tensile capacity of various steel cross-sections subjected to SMAW welding.

ISSN : 2541 - 0318 [Online]
ISSN : 2541 - 2884 [Print]

THEORY AND METHODS

Theory

The area surrounding a weld pool, known as the heat-affected zone (HAZ), is a critical region. During welding, the molten metal pool experiences very high temperatures. However, the adjacent HAZ also heats up significantly, without reaching a molten state. This intense heat alters the microstructure of the metal, which in turn affects its mechanical properties (Qi et al., 2024). Consequently, the HAZ often exhibits a decrease in strength and flexibility, while simultaneously becoming harder and more susceptible to cracking compared to the surrounding unaffected metal (Zhang et al., 2021).

Several factors influence the size and impact of the heat-affected zone (HAZ) surrounding a weld. Higher heat input during welding results in a larger and more impactful HAZ. The material properties also play a role. Thinner sections experience wider HAZ due to easier heat transfer compared to thicker sections. Finally, the type of welding method used makes a difference, since different methods generate varying amounts of heat.

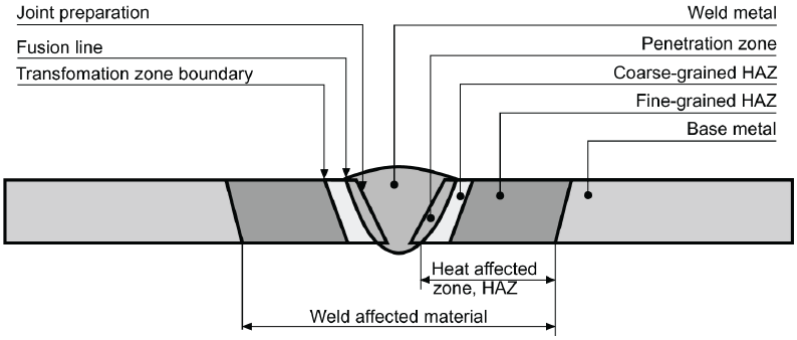

Figure 1. Heat-affected zone during welding (Weman, 2003)

A cross-section of a welded joint can be conceptually divided into two distinct regions: the heat-affected zone (HAZ) and the base metal (Figure 1). The capacity of a member to resist tension forces, known as its tensile strength, is influenced by more than just the intrinsic properties of the material itself.

The tension capacity of a steel section is a critical parameter in structural design, as it dictates the maximum tensile load the member can safely withstand. This capacity is primarily influenced by two key factors: the cross-sectional area of the steel and the material properties.

Firstly, the gross cross-sectional area, which represents the total area of the steel section, directly affects its tensile capacity. A larger cross-section can distribute the tensile load across a greater area, allowing it to bear a larger tensile load. However, engineers often utilize the effective net area for design purposes. This accounts for any holes or reductions in the section due to fabrication processes, providing a more realistic estimate of the available area to resist tension.

Secondly, the material properties of the steel, specifically its yield strength and tensile strength, play a crucial role. Yield strength represents the stress level beyond which the steel exhibits permanent deformation. The tensile capacity is often determined by a safety factor multiplied by the yield strength. Tensile strength, meanwhile, represents the maximum stress the steel can withstand before fracture. While it provides an ultimate limit, design considerations typically focus on yield strength to ensure the member remains elastic under normal operating conditions.

Methods

This study presents a numerical analysis investigating the impact of Shielded Metal Arc Welding (SMAW) on the tension capacity of commonly used hot-rolled angle sections. The analysis focuses on the thinnest readily available equal-leg angle sections commonly utilized in structural applications. These sections come in three sections 40.40.4, 50.50.5, and 60.60.6. The welding process employs the E6013 electrode, a popular selection for general-purpose SMAW applications (Denev, 2022).

Following the guidelines outlined in ASME Section IX (2021), equation (1) is employed to determine the heat input during the welding process.

$$HI = (V\ .\ A\ .60\ )/s \qquad (1)$$

In Equation (1), HI represents the heat input in kilojoules per millimeter (kJ/mm). V, A, and s correspond to the voltage (V), current (Amps), and welding speed (mm/min) employed during the welding process, respectively. As specified in EN ISO 1011-1 (2009) (Table 1), a thermal efficiency value of 0.8 is adopted for the SMAW process.

Table 1. Common thermal efficiency for each welding process

Welding process	Thermal efficiency
Submerged arc welding (SAW)	1.0
Shielded metal arc welding (SMAW)	0.8
Gas metal arc welding (GMAW)	0.8
Flux cored arc welding (FCAW)	0.8
Gas tungsten arc welding (GTAW)	0.6
Plasma arc welding (PAW)	0.6

These variations will produce different energy input (Hnet) values, as shown in Table 2 below.

ISSN : 2541 - 0318 [Online]
ISSN : 2541 - 2884 [Print]

Table 2. Welding parameter for each scenario

Scenario Num.	Diameter mm	Current amps	Voltage volts	Travel speed mm/min	Energy input kJ/mm
Scenario 1.1	3.2	75	35	75	1.680
Scenario 1.2				85	1.482
Scenario 1.3				95	1.326
Scenario 1.4				105	1.200
Scenario 1.5				115	1.096
Scenario 1.6				125	1.008
Scenario 1.7				135	0.933
Scenario 1.8				150	0.840
Scenario 2.1	3.2	85	35	75	1.904
Scenario 2.2				85	1.680
Scenario 2.3				95	1.503
Scenario 2.4				105	1.360
Scenario 2.5				115	1.242
Scenario 2.6				125	1.142
Scenario 2.7				135	1.058
Scenario 2.8				150	0.952
Scenario 3.1	3.2	95	35	75	2.128
Scenario 3.2				85	1.878
Scenario 3.3				95	1.680
Scenario 3.4				105	1.520
Scenario 3.5				115	1.388
Scenario 3.6				125	1.277
Scenario 3.7				135	1.182
Scenario 3.8				150	1.064
Scenario 4.1	3.2	105	35	75	2.352
Scenario 4.2				85	2.075
Scenario 4.3				95	1.875
Scenario 4.4				105	1.680
Scenario 4.5				115	1.534
Scenario 4.6				125	1.411
Scenario 4.7				135	1.307
Scenario 4.8				150	1.176
Scenario 5.1	3.2	115	35	75	2.576
Scenario 5.2				85	2.273
Scenario 5.3				95	2.034
Scenario 5.4				105	1.840
Scenario 5.5				115	1.680
Scenario 5.6				125	1.546
Scenario 5.7				135	1.431
Scenario 5.8				150	1.288
Scenario 6.1	3.2	125	35	75	2.800
Scenario 6.2				85	2.471
Scenario 6.3				95	2.211
Scenario 6.4				105	2.000
Scenario 6.5				115	1.826
Scenario 6.6				125	1.680
Scenario 6.7				135	1.556
Scenario 6.8				150	1.400

Table 3. Amperage range for E6013 type electrode

Electrode	Diameter		Amperage	Metal thickness	
	in	mm		in	mm
6013	1/16”	1.6	20-45	up to 1/8”	up to 3.2
6013	5/64”	2.0	35-60	up to 3/16”	up to 4.8
6013	3/32”	2.4	40-90	3/32 – 3/16”	2.4 – 4.8
6013	1/8”	3.2	80-130	1/8 – ¼”	3.2 – 6.4
6013	5/32”	4.0	105-180	¼” – 3/8”	6.4 – 9.5
6013	3/16”	4.8	150-230	over 3/8”	over 9.5
6013	7/32”	5.6	210-300	over 3/8”	over 9.5

ISSN : 2541 - 0318 [Online]
ISSN : 2541 - 2884 [Print]

The electrode diameter and corresponding current values were obtained from the manufacturer's product catalog (Table 3). A constant voltage of 35 V was utilized throughout the study. This voltage selection falls within the upper recommended limit for SMAW processes, prioritizing process stability and electrode life (Singh et al., 2013). Furthermore, it allows electrode diameter to be the primary factor influencing current and penetration depth. Since increasing voltage beyond this range is unlikely to offer substantial advantages in penetration depth for this application, a constant value was selected for consistency.

The selection of travel speeds for the welding process was informed by recommendations from various research studies and industry catalogs ((Nagesh & Datta, 2002), (Kumar et al., 2019), (Tadamalle & Reddy, 2020)). These sources consistently suggest a travel speed range of 3 to 6 inches per minute (75–150 mm/min) for SMAW applications.

In arc welding, thermal efficiency refers to the proportion of electrical energy delivered to the arc that contributes to heating the weld pool. While a nominal value of 0.8 is commonly adopted, several factors can influence the effectiveness of this energy transfer (Bassey et al., 2024).

A critical factor lies in the inherent variability of the heat source in SMAW compared to more controlled processes (Bassey et al., 2024). In SMAW, spatter and electrode resistance heating lead to less precise heat input and potential fluctuations in the amount of heat transferred to the workpiece (Murphy & Lowke, 2018). Travel speed and electrode size also play a role. Increased travel speeds or larger electrode diameters limit the time available for the arc to heat the metal, resulting in lower thermal efficiency.

Thermal efficiency is also influenced by material properties. Materials with higher thermal conductivity dissipate heat more readily, reducing the available energy for heating the weld pool. Finally, while machine settings have a minor influence, higher voltage settings can lead to a slight decrease in efficiency due to increased arc length. However, this effect is generally less significant compared to other factors, such as arc voltage and current (Ran et al., 2016), which as highlighted by Kah et al. (2014), play a key role in influencing arc efficiency in SMAW. Their research does not provide a single definitive value for SMAW, but emphasizes the importance of considering these parameters to achieve optimal welding results.

Table 4. Reduction factors for stress-strain relationship of steel at elevated temperatures (Lu et al., 2003)

Steel temperature θ_a	Reduction factors at temperature relative to the value at 20°C		
	Effective yield strength $k_{y,\theta} = f_{y,\theta} / f_y$	Proportional limit $k_{p,\theta} = f_{p,\theta} / f_y$	Slope of the linear elastic range $k_{E,\theta} = E_{a,\theta} / E_a$
20	1.000	1.0000	1.0000
100	1.000	1.0000	1.0000
200	1.000	0.8070	0.9000
300	1.000	0.6130	0.8000
400	1.000	0.4200	0.7000
500	0.780	0.3600	0.6000
600	0.470	0.1800	0.3100
700	0.230	0.0750	0.1300
800	0.110	0.0500	0.0900
900	0.060	0.0375	0.0675
1000	0.040	0.0250	0.0450
1100	0.020	0.0125	0.0225
1200	0.000	0.0000	0.0000

Note: For intermediate values of the steel temperature, linear interpolation may be used

Table 4 clearly demonstrates a correlation between increasing temperature and decreasing yield strength within a cross-section. To account for this variation, the study uses a segmented approach to analyze the cross-section. The section is divided into multiple groups based on yield strength. The first group encompasses the area with a yield strength of fy = 0. The remaining area is then further subdivided into smaller pieces, each categorized by yield strength values within a narrow range. This allows for a precise calculation of the effective cross-sectional area (A), as depicted in Figure 3, where the structural analysis software facilitates this area division process.

ISSN : 2541 - 0318 [Online]
ISSN : 2541 - 2884 [Print]

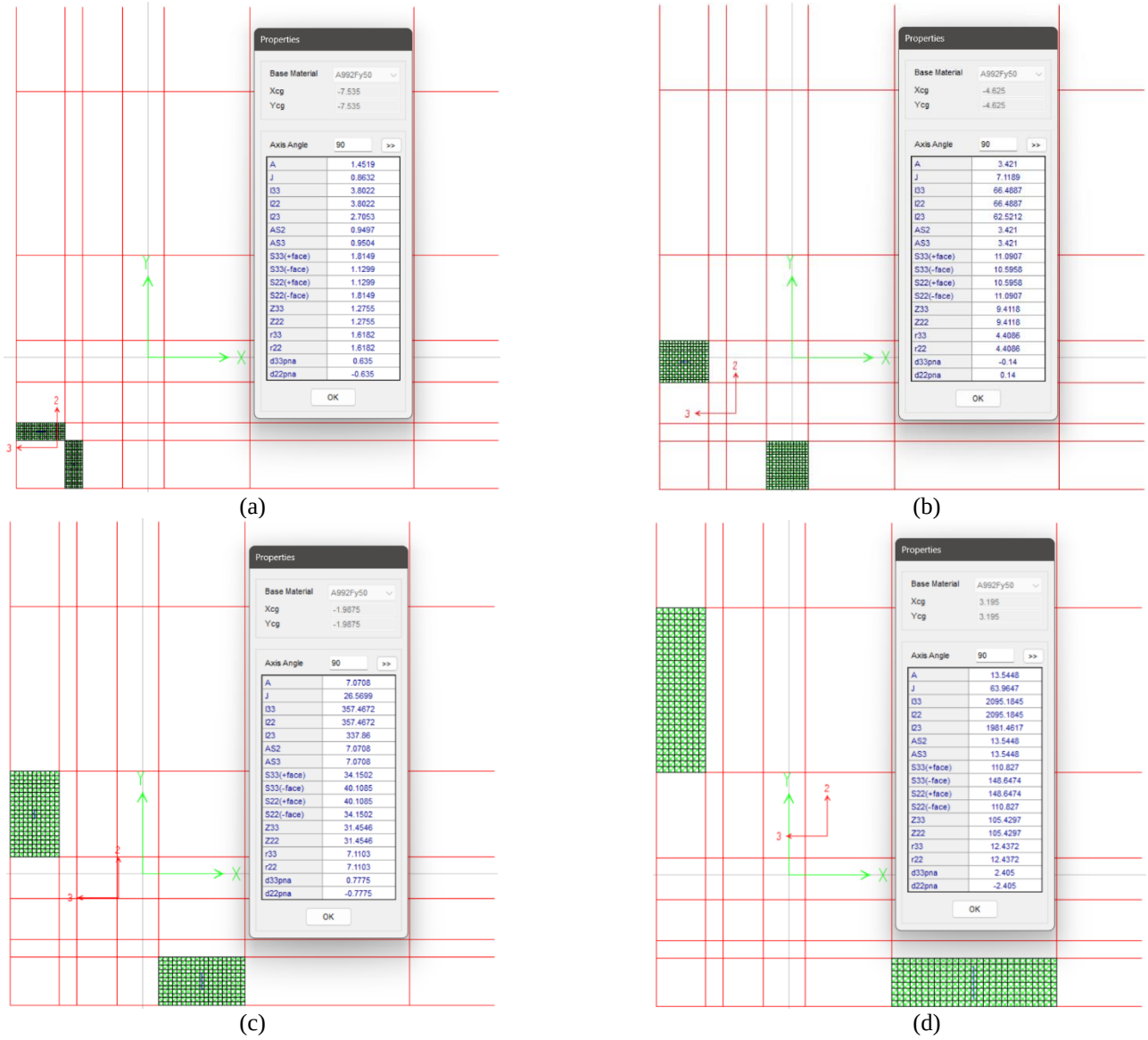

Figure 2. Property analysis across segments (a) to (d)

The section properties for each segment are calculated as shown in Figure 2. This allows for the evaluation of each segment's reduction in tension capacity. Subsequently, the total reduced tension capacity for the entire cross-section is obtained by summing the contributions from all segments. This process of evaluating individual segment capacity and calculating the total reduced capacity for the entire section is repeated for each welding simulation analyzed in the study.

The ultimate tension capacity of the heated section, accounting for strain hardening, was determined following Annex A of Eurocode EN 1993-1-2:2005 (E) as as shown by equation (2), (3) and (4):

- for temperatures, $\theta_a < 300^oC$
  $f_{u,\theta} = 1{,}25\ f_{y,\theta}$ (2)
- for $300^oC < \theta_a < 400^oC$
  $f_{u,\theta} = f_{y,\theta}\ (2 - 0{,}0025\ \theta_a)$ (3)
- for $\theta_a > 400^oC$
  $f_{u,\theta} = f_{y,\theta}$ (4)

The relationship between stress and strain, as it varies with temperature, is depicted in Figure 3.

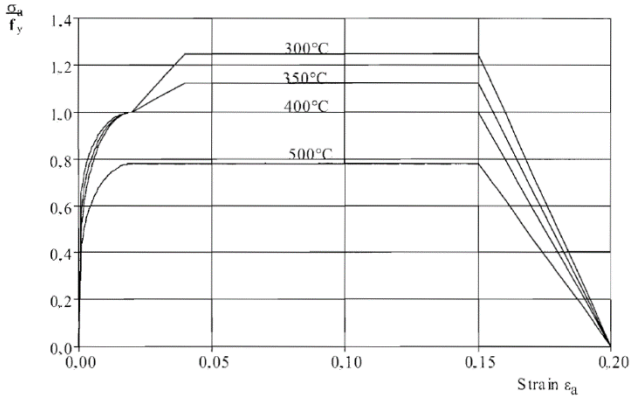

Figure 3. Stress-strain relationship of steel at elevated temperature (Eurocode, 2005)

ISSN : 2541 - 0318 [Online]
ISSN : 2541 - 2884 [Print]

RESULTS AND DISCUSSION

Simulation with various welding speeds (constant voltage and current)

This study utilized finite element models within simulations to calculate the remaining tension capacity of a member subjected to different welding speeds. It's important to note that these simulations were conducted while maintaining constant voltage and current values. The results revealed a noteworthy trend: a positive correlation between welding speed and the remaining tension capacity of the section.

As illustrated in Figure 4 (section 40.40.4), Figure 5 (section 50.50.5), and Figure 6 (section 60.60.6), the remaining tension capacity increases steadily as the welding speed is increased. This confirms an association between faster welding speeds (higher values) and a greater remaining tension capacity. Further research is needed to determine the existence of an optimal welding speed that maximizes the remaining tension capacity within the welded member.

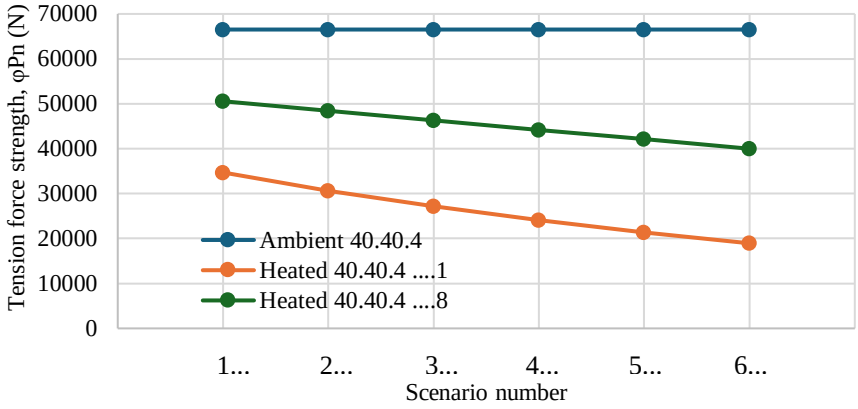

Figure 4. Tension capacity fluctuation to welding scenarios due to welding speed variation of 40.40.4 section

Table 5. Tension capacity fluctuation to welding scenarios due to welding speed variation of 40.40.4 section

Section	Scenario							
40.40.4	1.1	1.2	1.3	1.4	1.5	1.6	1.7	1.8
Heated	34708.01	39993.34	41390.18	43768.58	45731.70	47392.81	48808.52	50564.01
Ambient	66528.00	66528.00	66528.00	66528.00	66528.00	66528.00	66528.00	66528.00
Remaining	0.52	0.60	0.62	0.66	0.69	0.71	0.73	0.76
Reduction	0.48	0.40	0.38	0.34	0.31	0.29	0.27	0.24

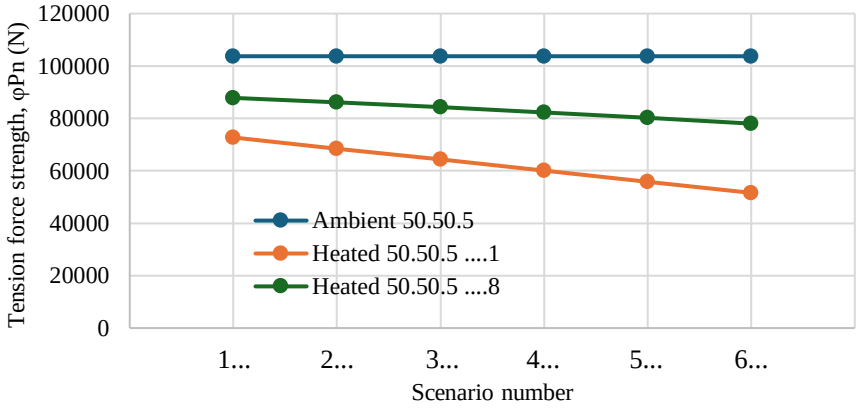

Figure 5. Tension capacity fluctuation to welding scenarios due to welding speed variation of 50.50.5 section

Table 6. Tension capacity fluctuation to welding scenarios due to welding speed variation of 50.50.5 section

Section	Scenario							
50.50.5	1.1	1.2	1.3	1.4	1.5	1.6	1.7	1.8
Heated	72733.01	78018.34	79415.18	81793.58	83756.70	85352.71	86462.42	87838.46
Ambient	103723.20	103723.20	103723.20	103723.20	103723.20	103723.20	103723.20	103723.20
Remaining	0.70	0.75	0.77	0.79	0.81	0.82	0.83	0.85
Reduction	0.30	0.25	0.23	0.21	0.19	0.18	0.17	0.15

ISSN : 2541 - 0318 [Online]
ISSN : 2541 - 2884 [Print]

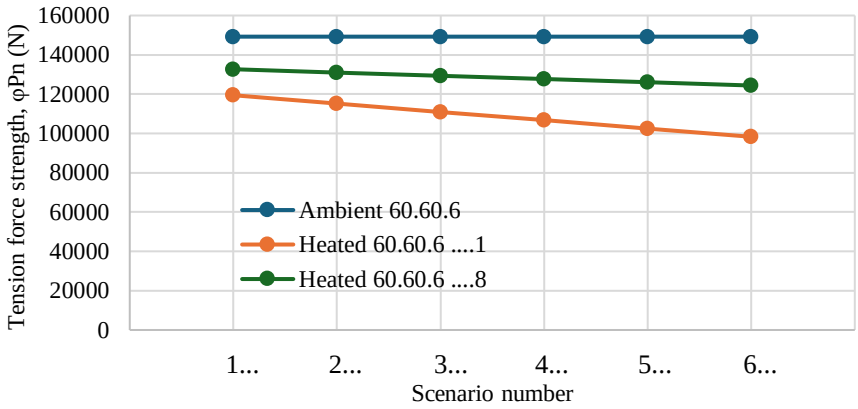

Figure 6. Tension capacity fluctuation to welding scenarios due to welding speed variation of 60.60.6 section

Table 7. Tension capacity fluctuation to welding scenarios due to welding speed variation of 60.60.6 section

Section	Scenario							
60.60.6	**1.1**	**1.2**	**1.3**	**1.4**	**1.5**	**1.6**	**1.7**	**1.8**
Heated	119443.01	124394.23	125489.14	127353.45	128892.25	130194.31	131304.02	132680.06
Ambient	149256.00	149256.00	149256.00	149256.00	149256.00	149256.00	149256.00	149256.00
Remaining	0.80	0.83	0.84	0.85	0.86	0.87	0.88	0.89
Reduction	0.20	0.17	0.16	0.15	0.14	0.13	0.12	0.11

A more comprehensive description of the findings is provided in Table 5 (for section 40.40.4), Table 6 (for section 50.50.5), and Table 7 (for section 60.60.6). These tables present the specific values of the remaining tensile strength across various welding speeds and section thicknesses. The simulations revealed a significant influence of section thickness on the remaining tensile strength. Notably, thinner sections experienced a greater reduction in tensile strength compared to thicker sections subjected to the same welding speeds. This trend is likely attributable to the increased heat concentration within thinner sections during the welding process. For instance, sections with a thickness of 4 mm exhibited reductions in tensile strength ranging from 24% to 48%, depending on the welding speed employed (as shown in Table 5). Conversely, sections with a thickness of 6 mm displayed a lower percentage loss, ranging from 11% to 20%.

Simulation with various currents (with constant voltage and constant welding speed)

The study also investigated the effect of welding current on the remaining tension capacity of welded members. Simulations were employed to analyze this relationship while maintaining constant voltage and welding speed values. The results revealed an opposite trend compared to the effect of welding speed. In this case, a negative correlation was observed between the welding current and the remaining tension capacity of the section.

As depicted in Figure 7, Figure 8, and Figure 9, the remaining tension capacity exhibits a clear decrease as the welding current is increased. This observation suggests that higher welding currents lead to a decrease in the member's ultimate tensile strength. This phenomenon can be attributed to the increased heat input associated with higher currents, which can potentially alter the microstructure and mechanical properties of the base metal and weld zone.

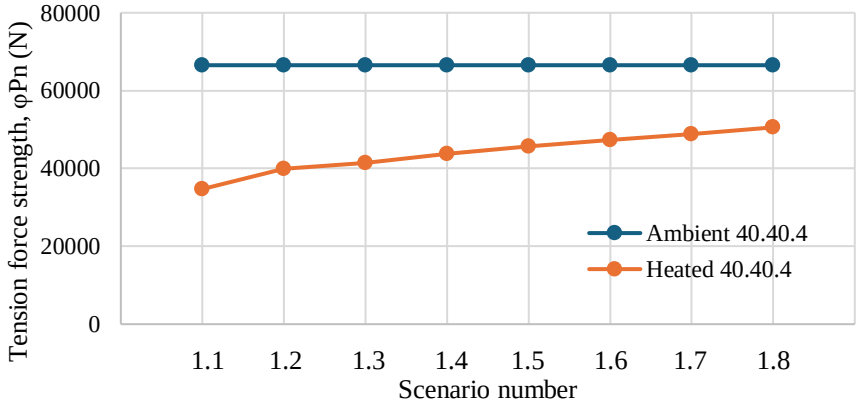

Figure 7. Tension capacity fluctuation to welding scenarios due to welding current variation of 40.40.4 section

Table 8. Tension capacity fluctuation to welding scenarios due to welding current variation of 40.40.4 section

ISSN : 2541 - 0318 [Online]
ISSN : 2541 - 2884 [Print]

Section	Scenario											
40.40.4	**1.1**	**1.8**	**2.1**	**2.8**	**3.1**	**3.8**	**4.1**	**4.8**	**5.1**	**5.8**	**6.1**	**6.8**
Heated	34708	50564	30647	48449	27220	46335	24135	44221	21373	42107	18939	39993
Ambient	66528	66528	66528	66528	66528	66528	66528	66528	66528	66528	66528	66528
Remaining	0.52	0.76	0.46	0.73	0.41	0.70	0.36	0.66	0.32	0.63	0.28	0.60
Reduction	0.48	0.24	0.54	0.27	0.59	0.30	0.64	0.34	0.68	0.37	0.72	0.40

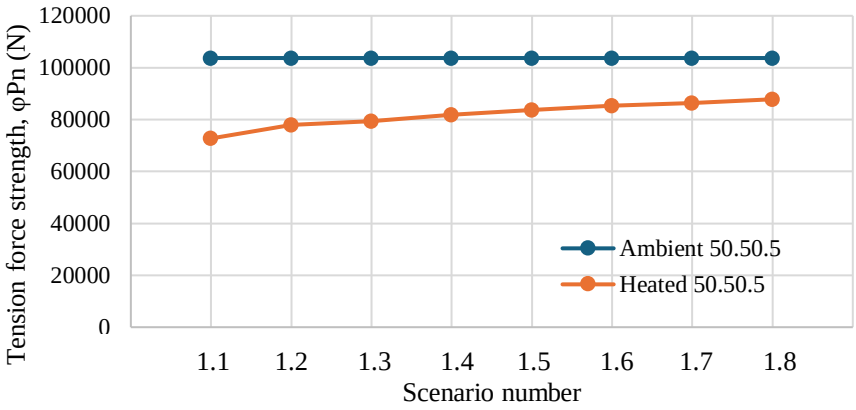

Figure 8. Tension capacity fluctuation to welding scenarios due to welding current variation of 50.50.5 section

Table 9. Tension capacity fluctuation to welding scenarios due to welding current variation of 50.50.5 section

Section	Scenario											
50.50.5	**1.1**	**1.8**	**2.1**	**2.8**	**3.1**	**3.8**	**4.1**	**4.8**	**5.1**	**5.8**	**6.1**	**6.8**
Heated	72733	87838	68504	86181	64276	84360	60048	82246	55819	80132	51591	78018
Ambient	103723	103723	103723	103723	103723	103723	103723	103723	103723	103723	103723	103723
Remaining	0.70	0.85	0.66	0.83	0.62	0.81	0.58	0.79	0.54	0.77	0.50	0.75
Reduction	0.30	0.15	0.34	0.17	0.38	0.19	0.42	0.21	0.46	0.23	0.50	0.25

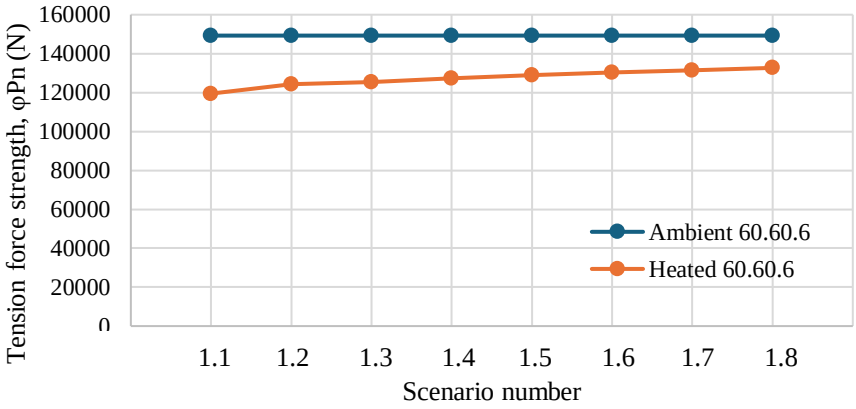

Figure 9. Tension capacity fluctuation to welding scenarios due to welding current variation of 60.60.6 section

Table 10. Tension capacity fluctuation to welding scenarios due to welding current variation of 60.60.6 section

Section	Scenario											
60.60.6	**1.1**	**1.8**	**2.1**	**2.8**	**3.1**	**3.8**	**4.1**	**4.8**	**5.1**	**5.8**	**6.1**	**6.8**
Heated	119443	132680	115214	131022	110986	129365	106758	127708	102529	126051	98301	124394
Ambient	149256	149256	149256	149256	149256	149256	149256	149256	149256	149256	149256	149256
Remaining	0.80	0.89	0.77	0.88	0.74	0.87	0.72	0.86	0.69	0.84	0.66	0.83
Reduction	0.20	0.11	0.23	0.12	0.26	0.13	0.28	0.14	0.31	0.16	0.34	0.17

Table 8 (for section 40.40.4), Table 9 (for section 50.50.5), and Table 10 (for section 60.60.6) provide a more in-depth analysis of the results, detailing the remaining tensile strength under varying welding currents and section

ISSN : 2541 - 0318 [Online]
ISSN : 2541 - 2884 [Print]

thicknesses. The simulations consistently revealed a significant influence of section thickness on the percentage loss of tension capacity. As observed previously, thinner sections exhibited a greater reduction in tensile strength compared to thicker sections subjected to the same welding currents. This trend is likely due to the increased heat concentration within thinner sections during the welding process, leading to more pronounced microstructural changes.

Thinner sections displayed a greater reduction in tensile strength compared to thicker sections under identical welding currents. This is evident by comparing sections welded with the lowest speed and highest current: a 4 mm section lost up to 72% of its tensile strength, whereas a 6 mm section only experienced a 34% loss (Tables 8-10). Interestingly, the welding speed also played a role. For a given section thickness, simulations using the lowest speed resulted in a loss of tension capacity nearly double that observed at the highest welding speed.

Impact of Welding Current and Welding Speed Variation

Welding current and speed significantly influence the remaining tension capacity of a welded section due to their impact on heat input. Higher welding currents inject a higher heat flux into the arc, resulting in a greater heat input into the base metal and weld zone. This intense heat can lead to several consequences related to microstructural changes and residual stresses. Due to microstructural changes, the high heat can alter the microstructure of the base metal and weld zone. Such changes include grain growth, which weakens the material (Digheche et al. 2017). Additionally, it can promote the formation of brittle phases, further reducing the section's ability to withstand tension load (Cui et al, 2014). From a residual stress perspective, uneven cooling during welding creates residual stresses within the joint. Higher heat input can worsen these stresses, potentially leading to cracking and reduced tension capacity (An et al., 2020).

Welding speed, on the other hand, is inversely related to heat input. Slower welding speeds allow more heat to be concentrated in a smaller area, similar to the effect of high welding currents. This concentration of heat can lead to similar detrimental effects observed with high welding currents, including detrimental microstructural changes in the base metal and weld zone, further weakening the section. Additionally, slower speeds can cause more localized heating, leading to greater thermal distortion in the member. This distortion can introduce stress concentrations and reduce the section's ability to resist tension (Tso-Liang et al., 2001).

Thinner sections are particularly sensitive to variations in welding current and speed due to their lower thermal capacity. This concentrated heat can lead to more severe microstructural changes and higher residual stresses, resulting in a more significant loss of tension capacity compared to thicker sections.

CONCLUSION

This study presented a method for calculating the remaining tension capacity of thin steel sections subjected to tensile forces during welding. The analysis employed simulations with various welding currents and speeds to investigate their influence on tension capacity. The results revealed a clear trend: higher welding currents resulted in a greater loss of tension capacity, while faster welding speeds led to a lesser loss.

Across all section thicknesses (40.40.4, 50.50.5, and 60.60.6), simulations revealed that the lowest welding current and fastest welding speed resulted in the minimal loss of tension capacity. In this scenario, the remaining tension capacity reached 76%, 85%, and 89% for the 40.40.4, 50.50.5, and 60.60.6 sections, respectively.

Conversely, employing the highest welding current and slowest welding speed resulted in a significant decrease in tension capacity. For the 40.40.4, 50.50.5, and 60.60.6 sections, the remaining tension capacity reached as low as 28%, 50%, and 66%, respectively.

REFERENCES

An, Gyubaek & Park, Jeongung & Han, Ilwook. (2020). Effects of High Toughness and Welding Residual Stress for Unstable Fracture Prevention. Applied Sciences. 10. 8613. 10.3390/app10238613.

American Society of Mechanical Engineers (ASME) Section IX (2021) the qualification standard for welding and brazing procedures.

Bassey, Michael & Ohwoekevwo, Jephtar & Ikpe, Aniekan. (2024). Thermal analysis of AISI 1020 low carbon steel plate agglutinated by gas tungsten arc welding technique: a computational study of weld dilution using finite element method. Journal of Engineering and Applied Science. 71. 1-22. 10.1186/s44147-024-00375-0.

Bi, Yueqi & Yuan, Xiaoming & Hao, Mingrui & Wang, Shuai & Xue, He. (2022). Numerical Investigation of the Influence of Ultimate-Strength Heterogeneity on Crack Propagation and Fracture Toughness in Welded Joints. Materials. 15. 3814. 10.3390/ma15113814.

British Standard BS EN 1011-1:2009 Welding — Recommendations for welding of metallic materials

Cui, D. & Lu, S. & Cui, Q. & Liu, B.. (2014). Effect of heat input on microstructure and mechanical properties of CMT welding-brazing joint between 5052 aluminum alloy and galvanized Q235 steel. Hanjie Xuebao/Transactions of the China Welding Institution. 35. 82-86.

Denev, Yordan. (2022). Analyze of Welding Arc Parameters In Shielded Metal Arc Welding. http://dx.doi.org/10.5281/zenodo.6884587.

Digheche, Keltoum & Boumerzoug, Z. & Malika, Diafi & Saadi, Khawla. (2017). Influence of heat treatments on the microstructure of welded API X70 pipeline steel. Acta Metallurgica Slovaca. 23. 72. 10.12776/ams.v23i1.879.

British Standard BS EN 1993-1-2:2005. Eurocode 3: Design of steel structures

Kah, Paul & Latifi, Hamidreza & Suoranta, Raimo & Martikainen, Jukka & Pirinen, Markku. (2014). Usability of arc types in industrial welding. International Journal of Mechanical and Materials Engineering. 9. 1-12. 10.1186/s40712-014-0015-6.

Kumar, Sudhir & Singh, Rajender. (2019). Investigation of tensile properties of shielded metal arc weldments of

ISSN : 2541 - 0318 [Online]
ISSN : 2541 - 2884 [Print]

AISI 1018 mild steel with preheating process. Materials Today: Proceedings. 26. http://dx.doi.org/10.1016/j.matpr.2019.10.167

Lozano M, Serrano MA, López-Colina C, Gayarre FL, Suárez J. The Influence of the Heat-Affected Zone Mechanical Properties on the Behaviour of the Welding in Transverse Plate-to-Tube Joints. Materials. 2018; 11(2):266. https://doi.org/10.3390/ma11020266

Murphy, Anthony & Lowke, John. (2018). Heat transfer in arc welding. http://dx.doi.org/10.1007/978-3-319-26695-4_29.

Mushthofa, Malik & Fakhri Pratama Nurfauzi, & Astriana Hardawati. (2023). Investigation of Effective Section Reduction in Low Carbon Steel during SMAW Welding. December 2023. Teknisia 28(2): 79-89. DOI: 10.20885/teknisia.vol28.iss2.art2

Nagesh, D.S. & Datta, G.L. (2002). Prediction of weld bead geometry and prediction in shielded metal-arc welding using artificial neural networks. Journal of Materials Processing Technology. 123. 303–312. 10.1016/S0924-0136(02)00101-2.

Parmar, Anil & Dubey, Aakash. (2017). Study of Heat Affected Zone for SMAW Process for Low Carbon Steel Specimen with controlled parameters. 10.21884/ijmter.2017.4339.cy2nc.

Qi, Huan, Qihang Pang, Weijuan Li, and Shouyuan Bian. (2024). "The Influence of the Second Phase on the Microstructure Evolution of the Welding Heat-Affected Zone of Q690 Steel with High Heat Input" Materials 17, no. 3: 613. https://doi.org/10.3390/ma17030613

Ran, Zong & Chen, J. & Wu, C.S. & Padhy, Girish. (2016). Influence of shielding gas on undercutting formation in gas metal arc welding. Journal of Materials Processing Technology. 234. 169-176. 10.1016/j.jmatprotec.2016.03.020.

Shaiful, Wan & Muda, Hasrizam & Syahida, Nurul & Nasir, Mohd & Mamat, Sarizam & Jamian, Saifulnizan. (2015). Effect of welding heat input on microstructure and mechanical properties at coarse grain heat affected zone of ABS grade a steel. ARPN Journal of Engineering and Applied Sciences. VOL. 10, NO 20, NOVEMBER, 2015. pg. 9487 - 9495

Singh, Rudra & Gupta, R.C. & Sarkar, S. (2013). Analysis of Depth of Penetration and Bead Width of Shielded Metal Arc Weld under Magnetic Field Applying Artificial Neural Networks. 10.13140/RG.2.2.25076.14722.

Tadamalle, Ashok & Reddy, Y.. (2020). Fatigue Life Prediction of Dissimilar Metal Laser Weld Joints. Journal of The Institution of Engineers (India): Series C. 101. http://dx.doi.org/10.1007/s40032-020-00603-5

Tso-Liang Teng, Chin-Ping Fung, Peng-Hsiang Chang, Wei-Chun Yang, (2001), Analysis of residual stresses and distortions in T-joint fillet welds, International Journal of Pressure Vessels and Piping, Volume 78, Issue 8, Pages 523-538, ISSN 0308-0161, https://doi.org/10.1016/S0308-0161(01)00074-6.

Weman, Klas. (2003). Welding processes handbook. Woodhead Pub.

Zhang, Yue, Jun Xiao, Wei Liu, and Aimin Zhao. (2021). "Effect of Welding Peak Temperature on Microstructure and Impact Toughness of Heat-Affected Zone of Q690 High Strength Bridge Steel" Materials 14, no. 11: 2981. https://doi.org/10.3390/ma14112981

Zhang, Zhuyao & Roberts, Steve & Wildgoose, Josh & Philpott, Will & Jepson, Mark. (2024). Effects of post-weld heat treatment on the microstructure and properties of the matching SMAW filler metal for weld joints in MarBN steel. Welding in the World. 10.1007/s40194-023-01653-w.